RSC Advances

COMMUNICATION

View Article Online
View Journal | View Issue

Cite this: *RSC Adv.*, 2016, **6**, 65594

Received 8th May 2016
Accepted 4th July 2016

DOI: 10.1039/c6ra11936k

www.rsc.org/advances

An easy method to modify PEDOT:PSS/perovskite interfaces for solar cells with efficiency exceeding 15%†

S. Shahbazi,[a] F. Tajabadi,*[b] H.-S. Shiu,[c] R. Sedighi,[d] E. Jokar,[c] S. Gholipour,[e] N. Taghavinia,*[de] S. Afshar[a] and E. W.-G. Diau[c]

Herein, we show that surface treatment of PEDOT:PSS films using propionic acid (PA) results in better device performance for the resulting $CH_3NH_3PbI_3$ perovskite solar cells (PCE > 15%). N_2 blow spreading of PA appears critical in enhanced performance. This weak acid treatment leads to no worse roughness, while providing larger perovskite grains.

Introduction

The field of photovoltaics based on perovskite solar cells has recently made remarkable progress owing to the excellent optical and electronic properties of the perovskite materials, such as strong absorption in the visible region and long charge carrier diffusion length.[1–5]

Efforts dedicated towards improving device architecture and optimization of perovskite film morphology have improved power conversion efficiency of PSCs up to 20%.[6–15] In conventional PSCs, a high-temperature thermal process is required for the metal oxide layers (titanium oxide and zinc oxide) used as the electron transport layer.[16–19] The high-temperature annealing is not consistent with the use of flexible plastic substrates.[20]

Inverted-type (planar) PSCs with a device structure of ITO/HTL/perovskite/ETL/metal have emerged as an alternative to conventional PSCs because of their low-temperature solution processability.[4,21,22] Most recently, PSCs based on planar structure also demonstrated remarkable efficiency over 12% by carrying out controllable interface engineering.[23–26] To date, most studies are focused on the perovskite film processing and relevant material design.[27–33] The perovskite light-absorbing layer is sandwiched between the hole- and electron-transporting layers in a typical planar PSC.[21] Thus, for pursuing high PCE cells, it is essential to manipulate the carrier behaviours in whole perovskite solar cell. Therefore, the interface control plays very important role for device optimization in planar PSCs.[34] Many hole transport layer (HTL) and electron transport layer (ETL) materials have been utilized to optimize the carrier transport pathway in the entire device. To date, different organic or inorganic HTLs such as poly(3,4-ethylene dioxythiophene):poly(4-styrenesulfonate) (PEDOT:PSS), poly-triarylamine derivatives, poly-diketopyrrolopyrrole derivatives, and 2,2,7,7-tetrakis (*N*,*N* dip-methoxyphenylamine)-9,9-spirobifluorene (spiro-OMeTAD), copper iodide (CuI), nickel oxide (NiO_x) and copper-doped nickel oxide (Cu:NiO_x) based PSCs have demonstrated promising PCEs.[35–42]

PEDOT:PSS is a commonly used HTL for indium tin oxide (ITO) modification in conventional organic solar cells.[43] Conducting polymer PEDOT:PSS has advantages of easy solution film-processing, high transparency and tuneable conductivity (10^{-4} to 10^{-3} S cm^{-1}). However the best efficiency for inverted-type PSCs with PEDOT:PSS as hole transport layer (HTL) is about 12–13% and modification of HTL or ETL (or both) are necessary for higher efficiency (more than 15%).[34,44,45] Different modification and treatments were reported for PEDOT:PSS HTL in perovskite solar cells including washing with different solvents, acid treatment and additives.[46,47] Modification may improve the perovskite film morphology, better energy level alignment, film conductivity and higher environment endurance. In the case of polar solvent treatment of PEDOT:PSS layer, the final PSC efficiency decreases, though the conductivity is enhance.[46] Gu *et al.* applied 3-aminopropanoic acid as a self-assembling monolayer (C3-SAM) on a PEDOT:PSS hole transport layer (HTL) to modify the crystallinity and coverage of the $CH_3NH_3PbI_{3-x}Cl_x$ film, resulting in much smoother perovskite surface morphology together with a PCE increase from 9.7% to

[a]*Department of Chemistry, Iranian University of Science and Technology, Tehran 16846-13114, Iran. E-mail: sh_afshar@iust.ac.ir*

[b]*Department of Nanotechnology and Advanced Materials, Materials and Energy Research Center, Karaj 3177983634, Iran. E-mail: f.tajabadi@merc.ac.ir*

[c]*Department of Applied Chemistry and Institute of Molecular Science, National Chiao Tung University, Hsinchu 30010, Taiwan. E-mail: diau@mail.nctu.edu.tw*

[d]*Faculty of Physics and Chemistry, Alzahra University, Tehran, 1993893973, Iran*

[e]*Institute for Nanoscience and Nanotechnology and Physics Department, Sharif University of Technology, Tehran 14588-89694, Iran. E-mail: taghavinia@sharif.edu*

† Electronic supplementary information (ESI) available: Photovoltaic parameters of 10 devises, contact angles, forward and reverse *J*–*V* curves, IPCE curve. See DOI: 10.1039/c6ra11936k

11.6%.[48] Recently GeO_2-doped PEDOT:PSS and Ag nanoparticles-doped PEDOT:PSS were reported for fabrication of invert-PSC with efficiency exceeding 15%.[49,50] Sun *et al.* reached the 15% power conversion efficiency with modification of hole and electron transport layers. They used methanesulfonic acid for treatment of PEDOT:SS film as hole transport layer and rhodamine 101 for modification of electron transport layer.[47]

In this study, we report an easy treatment method for fabrication of high-efficient inverted hetero-junction perovskite solar cell with just modification of hole transport layer. Here, we used the propionic acid (PA) for modification of PEDOT:PSS (HTL) using a gas assisted drop casting method. PA is a weak acid and is not corrosive toward PET surface so it is applicable for flexible solar cell fabrication. The increase in surface roughness after treatment with PA is relatively low. This eliminates the need for further roughness treatment. As previously reported, increase in PEDOT:PSS surfaces roughness results in lower cell efficiency.[47] Our results indicate that treatment of PEDOT–PSS with PA leads to improving of fill factor and device performance without any hysteresis. The resulting PSC device with PA treated hole transfer layer shows a best performance with 15.06% conversion efficiency.

Experimental section

Methylammonium iodide (CH_3NH_3I, MAI) was synthesized *via* the reaction of methylamine (CH_3NH_2, 21.6 mL, 40 mass% in water, Alfa Aesar) and hydriodic acid (HI, 30 mL, 57 mass% in water, with hypophosphorous acid 1.5%, Alfa Aesar) and stirred at 0 °C for 2 h under nitrogen atmosphere, followed by rotary evaporation to remove the solvent. The CH_3NH_3I powder was washed three times with diethyl ether (99%, anhydrous, ECHO) and dried in a vacuum oven at 50 °C overnight before use. To prepare the precursor solution, we mixed MAI and lead iodide (molar ratio 1 : 1) powders in anhydrous DMF with concentration 45% in mass proportion. The precursor solutions were stirred overnight at 70 °C and filtered through 0.45 μm PVDF membrane before device fabrication.

The etched ITO was cleaned with ultrasonic treatment in deionized water, acetone, propanol and UV ozone treatment was then performed. A thin film (PEDOT:PSS, AI4083, UR) was spin-coated on ITO substrates at a speed 5000 rpm for 50 s, then heated at 120 °C for 10 min. The PEDOT:PSS films were treated by 8 M propionic acid. The treatment with the acid was performed by dropping 70 μL of propionic acid on a PEDOT:PSS film on a hot plate at 120 °C and a dry nitrogen gas stream was blown over the PEDOT:PSS film to obtain a uniform film. The films were then dried on a hotplate at 120 °C for 8 min. To avoid oxygen and moisture, the substrates were transferred into N_2-filled glove box for deposition of the thin-film perovskite layers. The precursor solution was spread onto the ITO/PEDOT:PSS at a rate 5000 rpm for 15 s. After 4 s of spinning, chlorobenzene was injected onto the substrate. The total period of the annealing procedure was 10 min at 100 °C. After 2 min of annealing, 7 μL anhydrous DMF was injected around the substrates and then annealed for 8 min. PCBM (20 mg, FEM Tech) was dissolved in chlorobenzene (1 mL) and spin-coated on top of the perovskite layer at 1000 rpm for 30 s. The silver back-contact electrode was eventually deposited *via* thermal evaporation in a vacuum chamber.

The current–voltage characteristics were measured with a digital source meter (Keithley 2400) with the device under one-sun illumination (AM 1.5G, 100 mW cm^{-2}) from a solar simulator (XES-40S1, SAN-E1) calibrated with a standard silicon reference cell (VLSI Standards, Oriel PN 91150 V). (0.04 cm^2 cell surface area and 0.02 (V s^{-1}) scan rate). Incident photon to current conversion efficiency (IPCE) of the corresponding devices were recorded with a system consisting of a Xe lamp (PTiA-1010, 150W), a monochromator (PTi, 1200 g mm^{-1} blazed at 500 nm), and a source meter (Keithley 2400). X-ray diffraction (XRD) pattern was obtained on a X-ray diffractometer (BRUKER AXS, D8 Advance) using Cu K_α irradiation (λ = 1.5418 Å). Scanning electron micrographs (SEM) were recorded with a microscope (Hitachi SU-8010) to determine the morphology of the films. Absorption spectra were measured with a spectrophotometer (JASCO V-570). The surface morphology of the PEDOT films was characterized by atomic force microscopy (AFM) (VEECO-CP research). Contact angels were measured by a OCA 15 plus. The work functions were measured using Kelvin probe force microscopy (KPFM, Bruker).

Results and discussion

It has been reported that treatment of PEDOT:PSS films with a strong acid such as sulfuric acid or a mild acid such as methanesulfonic acid can improve its conductivity.[47,51] The film conductivity enhancement is due to PSS chains removing. However treatment of PEDOT:PSS with these acids result in more surface roughness (more than 2 folds) and lower hydrophilicity of surface. Here we used PA as a weak acid for treatment of PEDOT:PSS surface and studied its effect on the PVC properties. To investigate the influence of PA-treatment on perovskite crystallinity which is described schematically in Fig. 1, we performed X-ray diffraction (XRD) measurement. We prepared perovskite films on top of ITO glass substrates coated

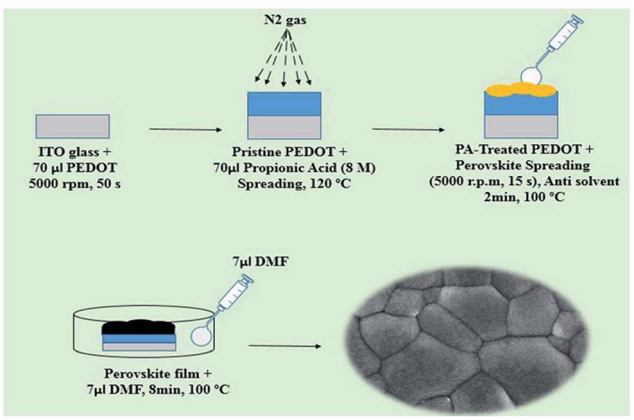

Fig. 1 Schematic of treatment of PEDOT:PSS with PA and deposition of perovskite film.

with PEDOT:PSS and PA-treated PEDOT:PSS. Both films exhibit diffraction peaks at 14.15°, 28.47° and 43.12°, corresponding to (110), (220) and (314) planes of the tetragonal perovskite phase (Fig. 2a). These peaks are consistent with XRD results in previous reports.[20,52] There is a small difference in the intensity of diffraction peaks, implying that perovskite film is crystallized almost the identically over both PEDOT:PSS and PA-treated PEDOT:PSS substrates.

There is no separate diffraction peak of PbI_2 in the XRD patterns of perovskite films after acid treatment similar to untreated surface that confirms total PbI_2 conversion into perovskite structure on both surfaces. The results indicate that the PA did not make negative effect on the crystal growth of perovskite film while the PbI_2 peaks appeared in the XRD patterns of perovskite films after treatment by some acids.[47]

Fig. 2b shows the UV-vis absorption spectra of the perovskite film deposited on PEDOT:PSS and PA-treated PEDOT:PSS. As can be seen, both films show a broad absorption, typical of the perovskite.[52] Both devices with treated and untreated PEDOT:PSS show similar absorption spectra over 400–800 nm.

Surface coverage and the morphology of perovskite film on the substrates are crucial for determining resultant performance of PSCs. To compare the morphology of perovskite films on PEDOT:PSS and PA-treated PEDOT:PSS, we utilized scanning electron microscopy (SEM). Fig. 3 shows that perovskite film formation with the solvent annealing method results in uniform free-pinhole surface with good surface coverage. The perovskite formation on PA-treated PEDOT:PSS layer leads to larger grain boundary compared to untreated PEDOT:PSS film. The cross-section images present crack-free perovskite layer for both untreated and treated PEDOT:PSS.

To further compare the surface property change of pristine and PA-treated PEDOT:PSS, we also studied the surface energy of them by performing contact angle measurements. Contact angles of pristine and PA-treated PEDOT:PSS to DMF solvent were 31.7° and 28.9°, respectively (Fig. S1, ESI†). This indicates that PEDOT:PSS layer treatment with PA leads to a small change in wettability. So both surfaces have similar interaction with DMF, PbI_2 and MAI. In previous reports where treatment led to more hydrophobic surface, an incomplete conversion of PbI_2 to perovskite occurs.[53] As shown in XRD patterns the conversion of PbI_2 to perovskite is complete for PA-treated PEDOT:PSS surface and similar to that of pristine surface.

Both pristine and PA-treated PEDOT:PSS layers provide uniform films with root-mean-square (r.m.s.) roughness of 1.4 nm and 1.6 nm respectively (AFM images, Fig. 4). AFM topography images are consistent with contact angle results. There is a small change in surface roughness after PA treatment, unlike many other acid treatments. We used N_2 gas flow for PA drying that may result in lower diffusion of PA solution into PEDOT:PSS film. Treatment of PEDOT:PSS surface with acids usually causes two-fold or more increase in the surface roughness.[47] In addition PA as a weak acid do not cause PET surface corrosion hence can be applied to flexible solar cells fabrication.

Fig. 5 presents current density–voltage (J–V) curves of best PSCs using pristine and PA-treated PEDOT:PSS as HTL. Devices

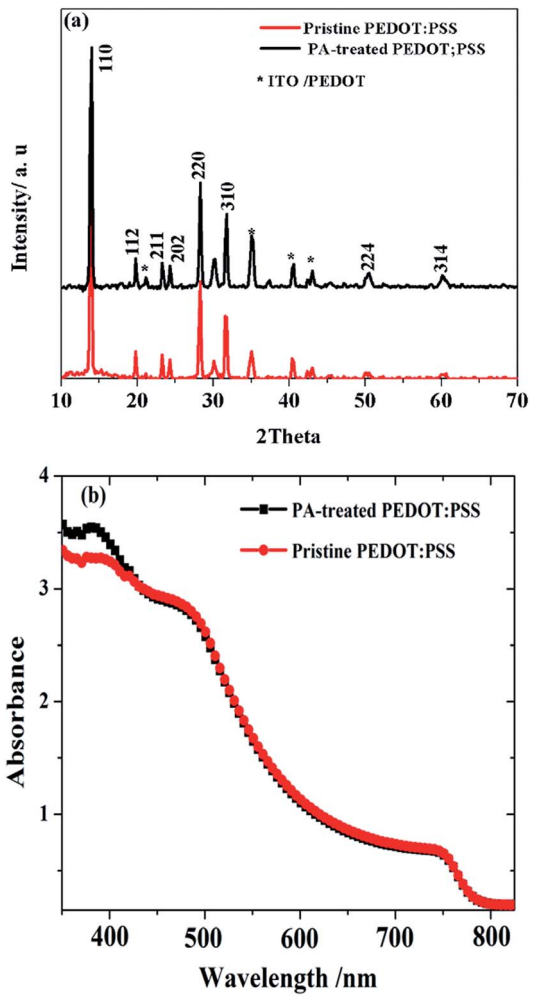

Fig. 2 XRD patterns (a) UV-vis spectra (b) of $MAPbI_3$ deposited on pristine PEDOT:PSS (red) and PA-treated PEDOT:PSS (black) surfaces.

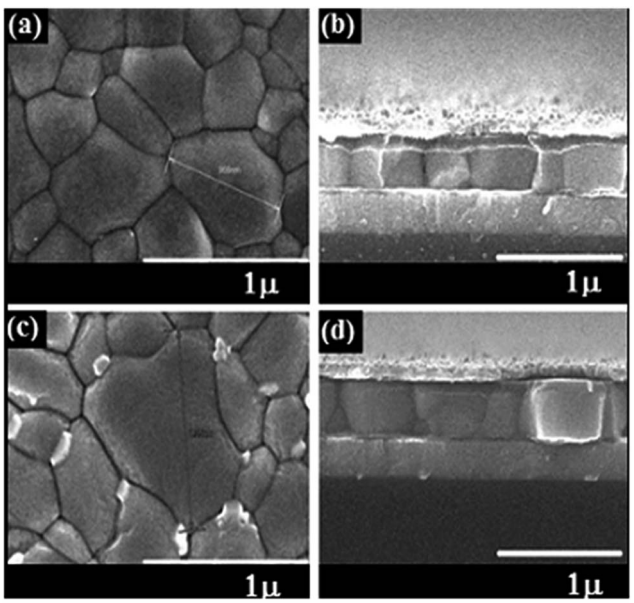

Fig. 3 SEM surface and cross-sectional images of perovskite films on (a, b) pristine PEDOT:PSS and (c, d) PA-treated PEDOT:PSS surface.

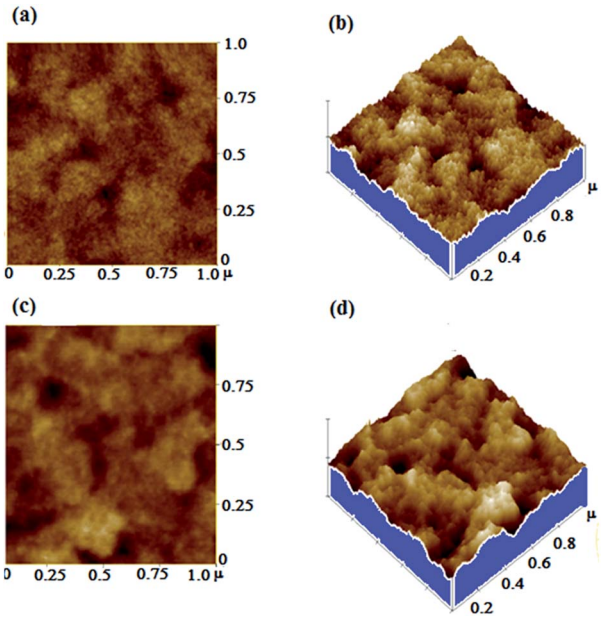

Fig. 4 AFM images of PEDOT:PSS films (a, b) untreated and treated (c, d) with 8 M propionic acid.

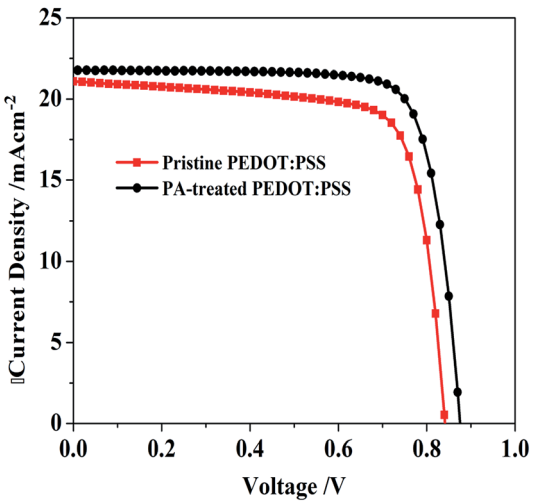

Fig. 5 *J–V* characteristics for PEDOT:PSS and PA-treated PEDOT:PSS based device.

with pristine PEDOT:PSS exhibited PCE of 13.37% with short-circuit current density (J_{SC}) of 21.09 mA cm^{-2}, open-circuit voltage (V_{OC}) of 0.84 V and fill factor (FF) of 0.75. Replacing pristine with PA-treated PEDOT:PSS led to a significant enhancement in device efficiency. The device yielded a PCE of 15.06% with J_{SC} of 21.75 mA cm^{-2}, V_{OC} of 0.88 V and FF of 0.78. The detailed solar cell parameters are listed in Table 1. From the *J–V* characteristics (Fig. 5 and Table 1), it is clear that the efficiency enhancement in the modified based devices was due mainly to the higher V_{OC} and FF.

The increase in V_{OC} can be attributed to reduce charge-carrier recombination in the absorber and treated HTL interface compared to untreated HTL. As it can be seen from SEM images, treatment of PEDOT:PSS results in perovskite deposition with larger grains that may lead to lower recombination.

Also as previously reported, acid treatment can affect the work function of PEDOT:PSS which in turn can affect the charge collection between PA-treated PEDOT and perovskite.[53] Fig. S2† shows the current–voltage hysteresis curves for the devices. As seen in this figure the hysteresis index for both devices is low. Fig. S3,† shows *J–V* and related external quantum efficiency curves for a device based PA-treated PEDOT:PSS. The J_{SC} of the devices with PA-treated PEDOT:PSS is consistent with the calculated J_{SC} from external quantum efficiency (EQE) curves.

To confirm the reproducibility of device performance, we tested 10 devices that were fabricated using PEDOT:PSS and PA-treated PEDOT:PSS. The photovoltaic parameters are reported in Tables 1 and 2S.† Average PCEs of the devices with PA-treated PEDOT:PSS (13.86%) were higher than those of the device with PEDOT:PSS (12.61%). Devices with PA-treated PEDOT:PSS exhibited higher V_{OC} (0.87 V) compared with devices based on PEDOT:PSS (V_{OC} = 0.84 V) whereas J_{SC} values for both devices are nearly the same. In the case of FF, the device with PA-treated PEDOT:PSS shows mainly higher values compared with pristine PEDOT:PSS based device (0.81 *vs.* 0.73).

For further investigation of PA treatment on the PEDOT:PSS properties, the work function values were measured (Fig. S4†). The Kelvin probe analysis demonstrates that work function of the pristine PEDOT:PSS is 5.2 eV, while the work function is reduced to 4.8 eV for the modified PEDOT:PSS. The lower work function is expected to increase the current density, while decreasing the open circuit voltage. We observe here that both J_{SC} and V_{OC} are improved after PA-treatment. In similar previously reported works[53] the work-function of PEDOT:PSS (5.0 eV) decreases after treatment with PA (4.8 eV). The increase in V_{OC} could be a result of improved interface and carrier transfer properties. Further studies are needed to clarify the effect of PA treatment on interface improvement.

In conclusion, we have successfully used PA for treatment of PEDOT:PSS HTL surface to enhance final cell conversion efficiency up to 15%. Treatment of PEDOT:PSS with PA only influences perovskite grain sizes and do not affect other film

Table 1 Photovoltaic device parameters of pristine PEDOT:PSS and PA-treated PEDOT:PSS based solar cells

Device		J_{SC}/mA cm^{-2}	V_{OC}/V	FF/%	η/%
Pristine PEDOT:PSS	Best	21.09	0.842	75.25	13.37
	Average	20.24 ± 1.00	0.844 ± 0.010	73.76 ± 3.20	12.61 ± 0.59
PA-treated PEDOT:PSS	Best	21.75	0.877	78.95	15.06
	Average	19.42 ± 0.70	0.870 ± 0.020	81.90 ± 1.54	13.86 ± 0.55

properties including film crystallinity, UV-vis absorption and surface roughness. Also treatment of PEDOT:PSS with PA leads to higher V_{OC} and fill factor compared to untreated device.

Notes and references

1 E. R. Dohner, A. Jaffe, L. R. Bradshaw and H. I. Karunadasa, *J. Am. Chem. Soc.*, 2014, **136**, 13154–13157.
2 L. Zhou, H. Y. Xiang, S. Shen, Y. Q. Li, J. D. Chen, H. J. Xie, I. A. Goldthorpe, L. S. Chen, S. T. Lee and J. X. Tang, *ACS Nano*, 2014, **8**, 12796–12805.
3 Z. K. Tan, R. S. Moghaddam, M. L. Lai, P. Docampo and R. Higler, *Nature*, 2014, **9**, 687–692.
4 J. You, Z. Hong, Y. Yang, Q. Chen, M. Cai, T.-B. Song, C.-C. Chen, S. Lu, Y. Liu, H. Zhou and Y. Yang, *ACS Nano*, 2014, **8**, 1674–1680.
5 Q. Dong, Y. Fang, Y. Shao, P. Mulligan, J. Qiu, L. Cao and J. Huang, *Science*, 2015, **347**, 967–970.
6 M. Xiao, F. Huang, W. Huang, Y. Dkhissi, Y. Zhu, J. Etheridge, A. Gray-Weale, U. Bach, Y.-B. Cheng and L. Spiccia, *Angew. Chem.*, 2014, **126**, 10056–10061.
7 Z. Zhou, Z. Wang, Y. Zhou, S. Pang, D. Wang, H. Xu, Z. Liu, N. P. Padture and G. Cui, *Angew. Chem.*, 2015, **54**, 9705–9709.
8 Q. Chen, H. Zhou, T.-B. Song, S. Luo, Z. Hong, H.-S. Duan, L. Dou, Y. Liu and Y. Yang, *Nano Lett.*, 2014, **14**, 4158–4163.
9 Z. Xiao, Q. Dong, C. Bi, Y. Shao, Y. Yuan and J. Huang, *Adv. Mater.*, 2014, **26**, 6503–6509.
10 T. Salim, S. Sun, Y. Abe, A. Krishna, A. C. Grimsdale and Y. M. Lam, *J. Mater. Chem. A*, 2015, **3**, 8943–8969.
11 G. E. Eperon, V. M. Burlakov, P. Docampo, A. Goriely and H. J. Snaith, *Adv. Funct. Mater.*, 2014, **24**, 151–157.
12 M. J. Carnie, C. Charbonneau, M. L. Davies, J. Troughton, T. M. Watson, K. Wojciechowski, H. Snaith and D. A. Worsley, *Chem. Commun.*, 2013, **49**, 7893–7895.
13 J. Burschka, N. Pellet, S.-J. Moon, R. Humphry-Baker, P. Gao, M. K. Nazeeruddin and M. Gratzel, *Nature*, 2013, **499**, 316–319.
14 D. Liu, L. Wu, C. Li, S. Ren, J. Zhang, W. Li and L. Feng, *ACS Appl. Mater. Interfaces*, 2015, **7**, 16330–16337.
15 N. Yantara, D. Sabba, F. Yanan, J. M. Kadro, T. Moehl, P. P. Boix, S. Mhaisalkar, M. Gratzel and C. Gratzel, *Chem. Commun.*, 2015, **51**, 4603–4606.
16 W. S. Yang, J. H. Noh, N. J. Jeon, Y. C. Kim, S. Ryu, J. Seo and S. I. Seok, *Science*, 2015, **348**, 1234–1237.
17 X. Gao, J. Li, J. Baker, Y. Hou, D. Guan, J. Chen and C. Yuan, *Chem. Commun.*, 2014, **50**, 6368–6371.
18 J.-W. Lee, T.-Y. Lee, P. J. Yoo, M. Gratzel, S. Mhaisalkar and N.-G. Park, *J. Mater. Chem. A*, 2014, **2**, 9251–9259.
19 K. Mahmood, B. S. Swain and A. Amassian, *Nanoscale*, 2014, **6**, 14674–14678.
20 C. Roldan-Carmona, O. Malinkiewicz, A. Soriano, G. Minguez Espallargas, A. Garcia, P. Reinecke, T. Kroyer, M. I. Dar, M. K. Nazeeruddin and H. J. Bolink, *Energy Environ. Sci.*, 2014, **7**, 994–997.
21 O. Malinkiewicz, A. Yella, Y. H. Lee, G. M. Espallargas, M. Graetzel, M. K. Nazeeruddin and H. J. Bolink, *Nat. Photonics*, 2014, **8**, 128–132.
22 P. Docampo, J. M. Ball, M. Darwich, G. E. Eperon and H. J. Snaith, *Nat. Commun.*, 2013, **4**, 2761.
23 Z. Zhou, S. Pang, Z. Liu, H. Xu and G. Cui, *J. Mater. Chem. A*, 2015, **3**, 19205–19217.
24 Z.-K. Wang, X. Gong, M. Li, Y. Hu, J.-M. Wang, H. Ma and L.-S. Liao, *ACS Nano*, 2016, **10**, 5479–5489.
25 Y. Hu, D.-Y. Zhou, B. Wang, Z.-K. Wang and L.-S. Liao, *Appl. Phys. Lett.*, 2016, **108**, 153303.
26 D.-X. Yuan, X.-D. Yuan, Q.-Y. Xu, M.-F. Xu, X.-B. Shi, Z.-K. Wang and L.-S. Liao, *Phys. Chem. Chem. Phys.*, 2015, **17**, 26653–26658.
27 P.-W. Liang, C.-Y. Liao, C.-C. Chueh, F. Zuo, S. T. Williams, X.-K. Xin, J. Lin and A. K. Y. Jen, *Adv. Mater.*, 2014, **26**, 3748–3754.
28 J. H. Heo, H. J. Han, D. Kim, T. K. Ahn and S. H. Im, *Energy Environ. Sci.*, 2015, **8**, 1602–1608.
29 F. Hao, C. C. Stoumpos, D. H. Cao, R. P. H. Chang and M. G. Kanatzidis, *Nat. Photonics*, 2014, **8**, 489–494.
30 F. Hao, C. C. Stoumpos, R. P. H. Chang and M. G. Kanatzidis, *J. Am. Chem. Soc.*, 2014, **136**, 8094–8099.
31 N. K. Noel, S. D. Stranks, A. Abate, C. Wehrenfennig, S. Guarnera, A.-A. Haghighirad, A. Sadhanala, G. E. Eperon, S. K. Pathak, M. B. Johnston, A. Petrozza, L. M. Herz and H. J. Snaith, *Energy Environ. Sci.*, 2014, **7**, 3061–3068.
32 Z.-K. Wang, M. Li, Y.-G. Yang, Y. Hu, H. Ma, X.-Y. Gao and L.-S. Liao, *Adv. Mater.*, 2016, DOI: 10.1002/adma.201600626.
33 X. Gong, M. Li, X.-B. Shi, H. Ma, Z.-K. Wang and L.-S. Liao, *Adv. Funct. Mater.*, 2015, **25**, 6671–6678.
34 Q. Xue, Z. Hu, J. Liu, J. Lin, C. Sun, Z. Chen, C. Duan, J. Wang, C. Liao, W. M. Lau, F. Huang, H.-L. Yip and Y. Cao, *J. Mater. Chem. A*, 2014, **2**, 19598–19603.
35 F. Zuo, S. T. Williams, P.-W. Liang, C.-C. Chueh, C.-Y. Liao and A. K. Y. Jen, *Adv. Mater.*, 2014, **26**, 6454–6460.
36 I. J. Park, M. A. Park, D. H. Kim, G. D. Park, B. J. Kim, H. J. Son, M. J. Ko, D.-K. Lee, T. Park, H. Shin, N.-G. Park, H. S. Jung and J. Y. Kim, *J. Phys. Chem. C*, 2015, **119**, 27285–27290.
37 L. Gil-Escrig, G. Longo, A. Pertegas, C. Roldan-Carmona, A. Soriano, M. Sessolo and H. J. Bolink, *Chem. Commun.*, 2015, **51**, 569–571.
38 C. Yi, J. Luo, S. Meloni, A. Boziki, N. Ashari-Astani, C. Gratzel, S. M. Zakeeruddin, U. Rothlisberger and M. Gratzel, *Energy Environ. Sci.*, 2016, **9**, 656–662.
39 Y. S. Kwon, J. Lim, H.-J. Yun, Y.-H. Kim and T. Park, *Energy Environ. Sci.*, 2014, **7**, 1454–1460.
40 G. A. Sepalage, S. Meyer, A. Pascoe, A. D. Scully, F. Huang, U. Bach, Y.-B. Cheng and L. Spiccia, *Adv. Funct. Mater.*, 2015, **25**, 5650–5661.
41 J.-Y. Jeng, K.-C. Chen, T.-Y. Chiang, P.-Y. Lin, T.-D. Tsai, Y.-C. Chang, T.-F. Guo, P. Chen, T.-C. Wen and Y.-J. Hsu, *Adv. Mater.*, 2014, **26**, 4107–4113.
42 J. H. Kim, P.-W. Liang, S. T. Williams, N. Cho, C.-C. Chueh, M. S. Glaz, D. S. Ginger and A. K. Y. Jen, *Adv. Mater.*, 2015, **27**, 695–701.
43 Z. Wu, S. Bai, J. Xiang, Z. Yuan, Y. Yang, W. Cui, X. Gao, Z. Liu, Y. Jin and B. Sun, *Nanoscale*, 2014, **6**, 10505–10510.

44 J. Seo, S. Park, Y. Chan Kim, N. J. Jeon, J. H. Noh, S. C. Yoon and S. I. Seok, *Energy Environ. Sci.*, 2014, **7**, 2642–2646.
45 Z. Zhao, Q. Wu, F. Xia, X. Chen, Y. Liu, W. Zhang, J. Zhu, S. Dai and S. Yang, *ACS Appl. Mater. Interfaces*, 2015, **7**, 1439–1448.
46 X.-Y. Li, L.-P. Zhang, F. Tang, Z.-M. Bao, J. Lin, Y.-Q. Li, L. Chen and C.-Q. Ma, *RSC Adv.*, 2016, **6**, 24501–24507.
47 K. Sun, P. Li, Y. Xia, J. Chang and J. Ouyang, *ACS Appl. Mater. Interfaces*, 2015, **7**, 15314–15320.
48 Z. Gu, L. Zuo, T. T. Larsen-Olsen, T. Ye, G. Wu, F. C. Krebs and H. Chen, *J. Mater. Chem. A*, 2015, **3**, 24254–24260.
49 M. Qian, M. Li, X.-B. Shi, H. Ma, Z.-K. Wang and L.-S. Liao, *J. Mater. Chem. A*, 2015, **3**, 13533–13539.
50 Z.-K. Wang, M. Li, D.-X. Yuan, X.-B. Shi, H. Ma and L.-S. Liao, *ACS Appl. Mater. Interfaces*, 2015, **7**, 9645–9651.
51 Y. Xia, K. Sun and J. Ouyang, *Adv. Mater.*, 2012, **24**, 2436–2440.
52 K.-G. Lim, H.-B. Kim, J. Jeong, H. Kim, J. Y. Kim and T.-W. Lee, *Adv. Mater.*, 2014, **26**, 6461–6466.
53 K. Sun, P. Li, Y. Xia, J. Chang and J. Ouyang, *ACS Appl. Mater. Interfaces*, 2015, **7**, 15314–15320.